JTTEE5 22:433–440
DOI: 10.1007/s11666-012-9849-8
1059-9630/$19.00 © ASM International

Impacting Behavior of Large Oxidized Copper Particles in Cold Spraying

Min Yu, Wenya Li, Xueping Guo, and Hanlin Liao

(Submitted June 25, 2012; in revised form October 12, 2012)

In a previous study, it has been experimentally demonstrated that surface oxide films of metallic particles have significant influence on the properties of cold-sprayed coatings. To clearly reveal the underlying mechanism, this study focused further on the effect of particle oxidation on the deposition behavior of oxidized Cu powder. Results show that the presence of the oxide films on the particles' surface can inhibit the plastic deformation of the particles. In addition, results concerning the morphologies and oxygen content of the rebounded particles show that the particles have experienced large plastic deformation that results in the break-up of the oxide films during the impacting process. Correspondingly, the hardness of the coating deposited with the oxidized powder is a little lower than that with the annealed powder because of the inferior plastic deformation and strain-hardening effect.

Keywords cold spray, deformation behavior, microhardness, oxide films, oxidized Cu powder

1. Introduction

In cold spraying (CS), solid powder particles are injected into a gas stream at the inlet of a converging/diverging de-Laval-type nozzle to attain a high velocity before impacting upon a substrate, and coatings are formed under the intensive plastic deformation of particles at a temperature well below the melting point of spray materials (Ref 1-3). It has been widely accepted that, for a given material, there exists a critical velocity greater than which a transition from erosion to deposition occurs. The critical velocity is associated with the properties of spray materials (Ref 1), the particle size and particle temperature (Ref 4-6), and the particle surface oxidation state (Ref 7-9). It has been reported that the oxidation condition of the starting powder has a significant effect on the critical velocity. Different critical velocities for Cu particles measured in experiments have been reported: 570 m/s (Ref 10), 550 m/s (Ref 11), and 640 m/s (Ref 12) with the oxygen contents of 0.1, 0.2, and 0.336 wt.%, respectively. In addition, the critical velocities of 610, 550, and 310 m/s with the oxygen contents of 0.38, 0.14, and 0.02 wt.%, respectively, were also reported through combining a theoretical model with the experiments (Ref 5, 13). The discrepancy in the critical velocity was attributed to different oxygen contents of the sprayed Cu powders (Ref 5). Both Kang et al. (Ref 8) and Li et al. (Ref 13) further concluded that higher feedstock oxygen content would lead to higher critical velocity.

Our previous study (Ref 9) demonstrated that the surface oxide films of metallic particles had a significant influence on the deposition efficiency, the microstructure, and the properties of cold-sprayed coatings, for example, the oxidation inclusions at the interfaces could greatly inhibit the effective bonding and lower the bonding strength between the coating and substrate (Ref 9). This study further focused on the effect of particle's oxidation on the particle deposition behavior to clearly reveal the underlying reasons.

Here, it should be noted that large gas-atomized Cu powder was sieved and artificially oxidized, because the dependency of the critical velocity on the particle size becomes weak for relatively large particles (Ref 6). Thus the variation in the critical velocity and the coating microstructure described in the following sections would not be the result of a change in the particle size but the presence of the oxide films. Moreover, the use of relatively large particles is beneficial to obtain a better observation for revealing the impact behavior.

This article is an invited paper selected from presentations at the 2012 International Thermal Spray Conference and has been expanded from the original presentation. It is simultaneously published in *Thermal Spray 2012: Proceedings of the International Thermal Spray Conference, Air, Land, Water, and the Human Body: Thermal Spray Science and Applications,* Houston, Texas, USA, May 21-24, 2012, Basil R. Marple, Arvind Agarwal, Laura Filofteia-Toma, Margaret M. Hyland, Yuk-Chiu Lau, Chang-Jiu Li, Rogerio S. Lima, and André McDonald, Ed., ASM International, Materials Park, OH, 2012.

Min Yu, State Key Laboratory of Solidification Processing, Shaanxi Key Laboratory of Friction Welding Technologies, Northwestern Polytechnical University, Xi'an 710072, PR China; and LERMPS, Université de Technologie de Belfort-Montbéliard Site de Sévenans 90010 Belfort Cedex, France; **Wenya Li,** State Key Laboratory of Solidification Processing, Shaanxi Key Laboratory of Friction Welding Technologies, Northwestern Polytechnical University, Xi'an 710072, PR China; **Xueping Guo,** Marine Engineering College, Jimei University, Xiamen, Fujian, China; and **Hanlin Liao,** LERMPS, UniversitÕ de Technologie de Belfort-MontbÕliard, Site de SÕvenans, 90010 Belfort Cedex, France.Contact e-mails: liwy@nwpu.edu.cn ,and min.yu@utbm.fr.

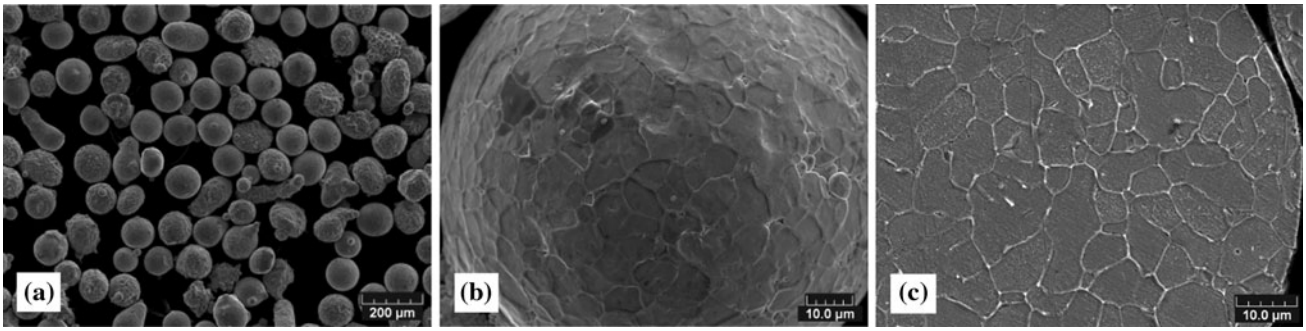

Fig. 1 SEM morphologies of the starting Cu powder (a), a particle (b), and cross section of a particle (c)

2. Materials and Experimental Procedures

The sieved gas-atomized Cu powder (−120+150 mesh, LERMPS Lab, France) was selected as the feedstock powder as shown in Fig. 1. The starting Cu particles present a spherical morphology with equiaxed grains having a size of the order of ten micrometers (see Fig. 1c). Some powder was oxidized at 250 °C for 4 h in a resistance furnace. The powder size distribution was characterized by a laser diffraction sizer (MASTERSIZER 2000, Malvern Instruments Ltd., UK). Cold-rolled Cu plates were polished as substrates, and some plates experienced the same oxidation procedure as the powder.

A cold-spray system with a commercial cold-spray gun (CS-3000, CGT GmbH, Germany) was employed for coating deposition. A nozzle with an expansion ratio of about 4.9 and a divergent section length of 170 mm was adopted. High-pressure compressed air was used as the accelerating gas at a pressure of 2.7 MPa and temperature of about 513 °C. Argon was used as the powder carrier gas at a pressure of 2.9 MPa. The standoff distance from the nozzle exit to the substrate surface was 30 mm.

Microstructures of the powder and coatings were examined by optical microscope (OM, Nikon, Japan) and scanning electron microscope (SEM, JSM5800LV, JEOL, Japan). Some cross-sectional samples were etched with an aqueous solution composed of 5 g $FeCl_3$ + 10 mL HCl + 100 mL H_2O. The microhardness was tested by a Vickers hardness indenter (Leitz, Germany) with a load of 300 g for the coatings and a load of 100 g for the particles.

3. Results and Discussion

3.1 Powder Characterizations

The particle size distribution and morphology of the oxidized Cu powder are shown in Fig. 2 and 3, respectively. The particle size of the oxidized Cu powder is in the range of 48.5-131.7 μm with an average size of 81.4 μm. The oxidized powder (Fig. 3a) retains the spherical morphology of the starting Cu powder. After the oxidation process, the oxygen content was increased from 0.17 wt.% in the starting powder to 0.63 wt.% in the oxidized powder. It can be found that oxide films cover the particle

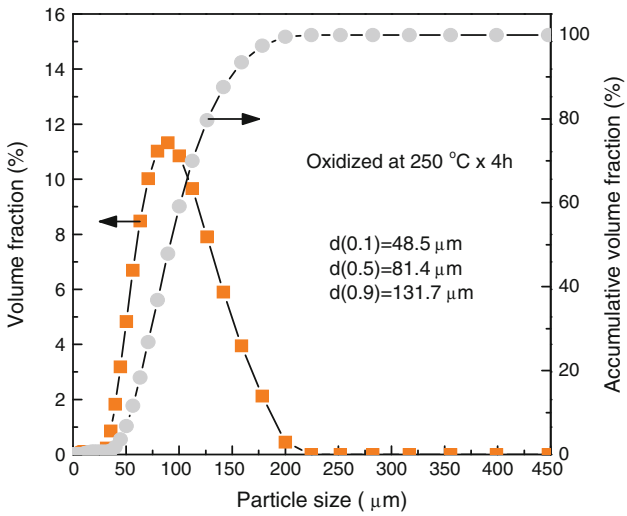

Fig. 2 Size distribution of the oxidized Cu particles

surfaces with a thickness of about several micrometers (see Fig. 4). Some of the oxide films have peeled off as shown in Fig. 3(b), and some have remained intact (see Fig. 3c) during the oxidation process. The composition of the oxide films has been verified as Cu_2O, based on the electron diffraction (SAED) (Ref 9). Cross sections of the oxidized Cu particles are shown in Fig. 4. It also can be seen from Fig. 4(b) that the oxide films are around the Cu particles. After etching, the oxidized Cu particles present the same equiaxed grains as the starting Cu particles (see Fig. 4d).

To initially estimate the depositability of the oxidized Cu powder, a developed 2D axisymmetrical model using the FLUENT software (Ref 14) was employed to calculate the particle velocity, and simulated results are shown in Fig. 5. It is clearly seen that the velocity of the oxidized particles ranges from 300 to 420 m/s with the average velocity of 357 m/s at the gas condition of 513 °C/2.7 MPa. As the critical velocity for bonding is size dependent, according to the equation, $v_{\text{crit}}^{\text{Cu}} = 900 \cdot d_{\text{particle}}^{-0.19}$ (Ref 6), the critical velocity of the present powder ranges from 356.1 to 430.5 m/s with the average velocity of 390.1 m/s. It seems that the particle velocity in the present study will be satisfactory for the deposition of part of the oxidized Cu

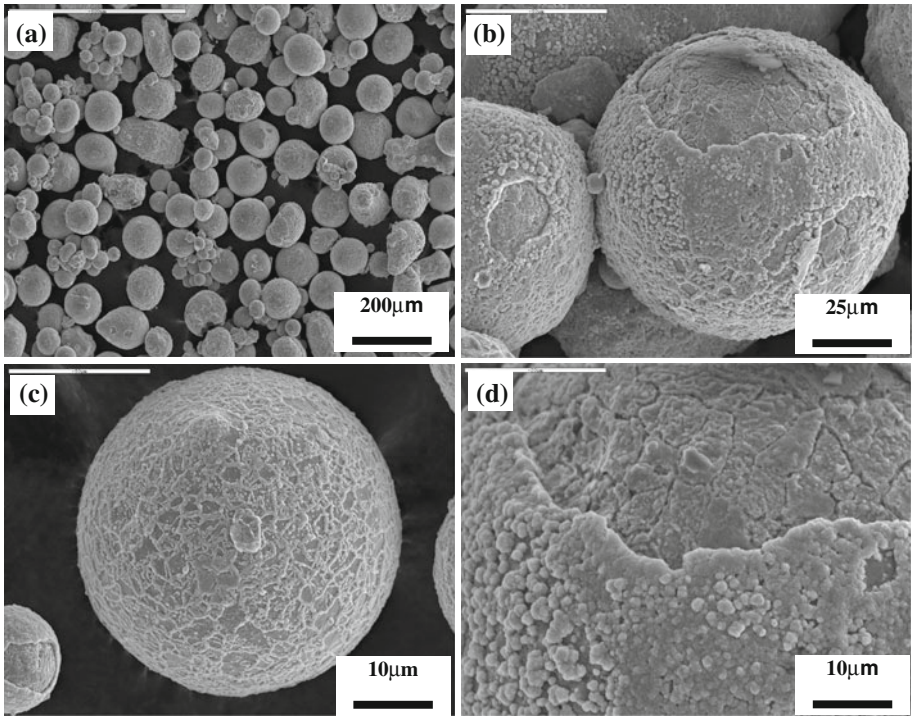

Fig. 3 SEM morphologies of the oxidized Cu powder (a, b) and a particle (c, d)

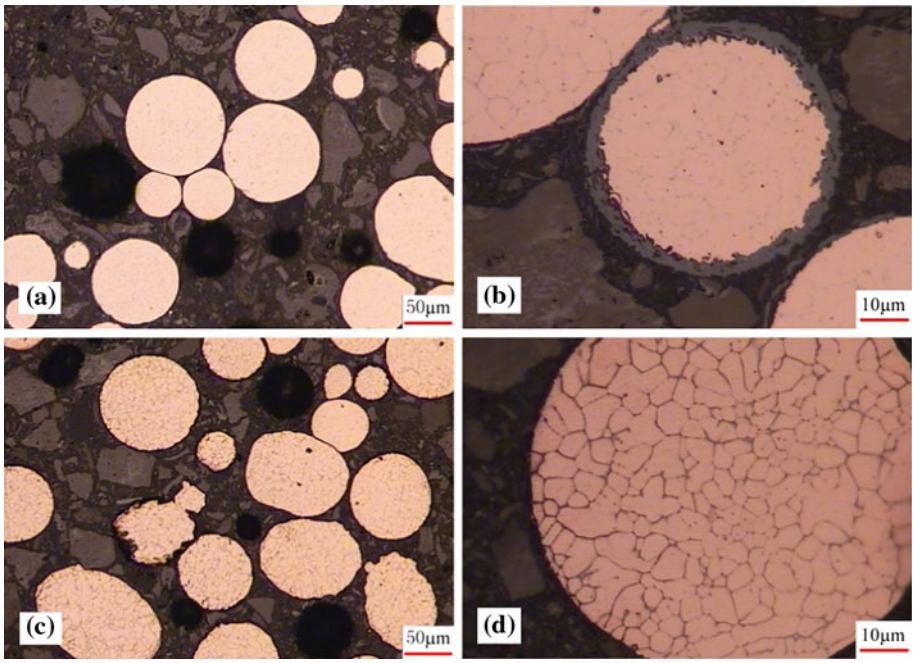

Fig. 4 Micrographs of cross sections of the oxidized Cu powder before (a, b) and after (c, d) etching

particles; however, as mentioned in the introduction, the critical velocity greatly depends on the oxidation condition of the sprayed powder, and higher feedstock oxygen content would lead to higher critical velocity. Therefore, the velocity of the oxidized Cu powder at the gas condition of 513 °C/2.7 MPa could be insufficient, and the depositability of the present oxidized Cu powder should be assessed by the experiments.

3.2 Particle Impact Behavior

3.2.1 The Rebounded Particles. According to the previous study (Ref 15), a coating could be formed using the large annealed Cu powder at the gas condition of 513 °C/2.7 MPa, but it was very difficult to form a coating with the oxidized Cu powder at the same gas condition. To explore the reason from the viewpoint of particle impacting behavior, the rebounded oxidized Cu particles were collected after a single impact test at the gas condition of 513 °C/2.7 MPa. SEM morphologies of the collected annealed Cu (Ref 15) and oxidized Cu particles are shown in Fig. 6. By carefully comparing the two morphologies, it can be seen that the annealed Cu particles have experienced large plastic deformation to form a lens-like shape, as indicated by the zones marked by the circles in Fig. 6(c), while the oxidized particles have been less flattened and some particles were approximately spheroidal, marked by the white arrow shown in Fig. 6(e). These results suggest that the oxide films could obstruct the particle deformation, and crushing the oxide films could dissipate part of the kinetic energy. Therefore, more kinetic energy should be provided to obtain a sound particle deformation, and the gas condition for deposition of the oxidized powder was adjusted to be 640 °C/2.5 MPa, which can yield the same particle velocity but higher particle temperature. It has been reported that the critical velocity decreases with the increase of particle temperature (Ref 3, 16). Characterization of the sprayed particles and coatings was summarized in Table 1. It can be found that under higher-temperature gas condition, the oxidized Cu coatings could be deposited but still with a thinner coating compared with the coating deposited with the annealed powder. SEM morphology of the collected oxidized Cu powder at the gas condition of 640 °C/2.5 MPa is shown in Fig. 7. Evidence of a larger deformation can be clearly observed as compared with the morphologies of the collected oxidized Cu powder at 513 °C/2.7 MPa (see Fig. 6d-f). The average particle size of the collected oxidized particles at 640 °C/2.5 MPa is about 113.8 μm

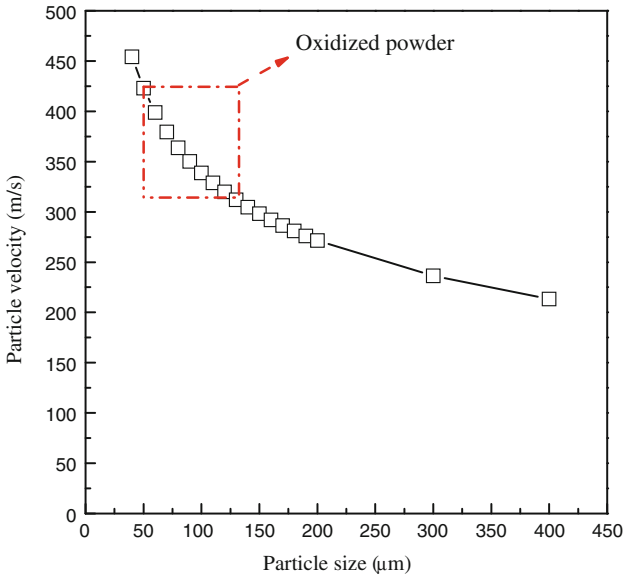

Fig. 5 Calculated particle velocity before impact with the developed 2D model using FLUENT (Ref 14). Note that the frame in this figure stands for the particle size and velocity windows, and the gas condition is 513 °C/2.7 MPa

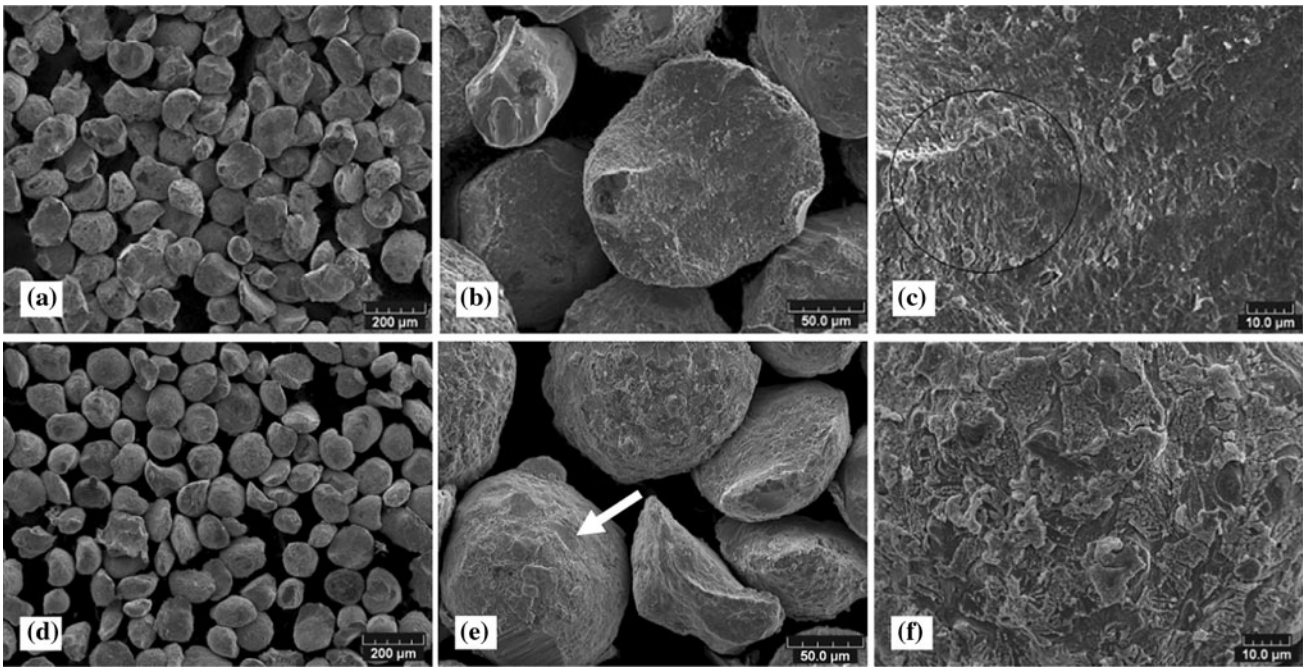

Fig. 6 SEM morphologies of the annealed Cu powder (a, b, c) (Ref 15) and oxidized Cu powder (d, e, f) collected after a single impact at 513 °C/2.7 MPa

Table 1 Comparison of characterization between the annealed Cu (Ref 15) and oxidized Cu particles

Particle	Average size before spaying, μm	Particle hardness, $HV_{0.1}$	Gas condition. °C/MPa	Calculated velocity, m/s	Particle size collected, μm	Coating thickness, μm
Annealed Cu	99.1	59.5	513/2.7	340	121.1	~350
Oxidized Cu	81.4	64.4	513/2.7	357	No collection	~0
			640/2.5	~357	113.8	~300

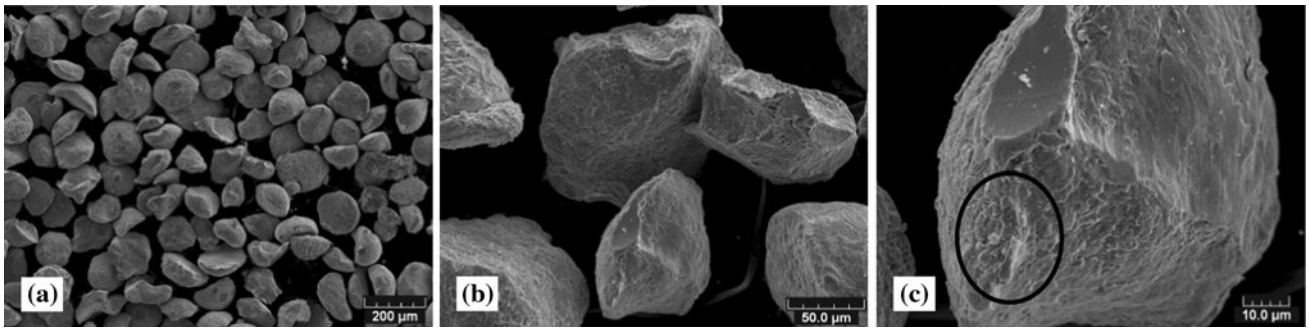

Fig. 7 SEM morphologies of oxidized Cu powder (a, b) and a particle (c) collected after coating deposition at 640 °C/2.5 MPa

compared to the average size of about 81.4 μm for the starting oxidized particles (see Table 1). This increase in the particle size could have arisen for two main reasons. One is the flattening of the impacted particles (see Fig. 7), and the other is that the relatively small particles took precedence over the large ones in deposition, and thus the large particles could have rebounded. By comparing the size distribution of the collected oxidized Cu powder shown in Fig. 8 with the size distribution of the starting oxidized Cu powder shown in Fig. 2, it can be seen that the peak of the volume fraction of the collected oxidized Cu powder is higher than that of the starting oxidized Cu powder, which illustrates that the particle size of the collected oxidized Cu powder concentrated in a narrower range, and thus the second reason is proven. In addition, measurements of the oxygen content show that the oxygen content of the collected powder after deposition at the gas condition of 640 °C/2.5 MPa is 0.23 wt.% compared to 0.63 wt.% of the starting oxidized powder. The results suggest that the rebounded particles have experienced large plastic deformation that results in the break-up of the oxide films during the impacting process. This fact also reflects the interface cleaning mechanism via the plastic deformation.

3.2.2 Morphology Characterization of the Coatings. Figure 9 shows the representative micrographs of the oxidized Cu particles after the single impact at 513 °C/2.7 MPa. As mentioned before, it was hard to obtain a coating at this gas condition (see Table 1). Correspondingly, few oxidized particles adhered to the substrate, and craters caused by particle impact were widely distributed on the substrate. The interface between the adhered particles and the substrate can be clearly distinguished when observed at high magnification, as shown in Fig. 9(b). In addition, the cross section (see Fig. 9c) also presents a distinguishable interface, which usually means a weak bonding.

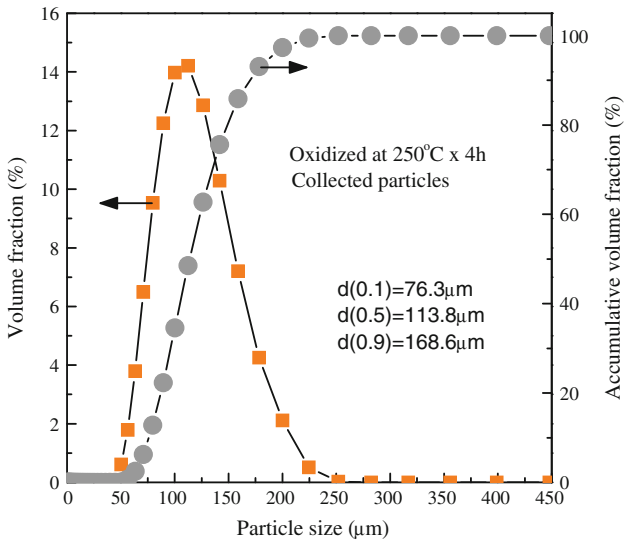

Fig. 8 Size distribution of the collected oxidized Cu powder after coating deposition at 640 °C/2.5 MPa

Figure 10 shows the surface morphology of the deposited oxidized Cu coating at the gas condition of 640 °C/2.5 MPa. The upper surface presents a deformed and irregular shape as shown in Fig. 10(b) and (c). For coating deposition, the successive impacting of the subsequent particles enhances the coatings. Some representative micrographs of cross sections of the oxidized Cu coatings are shown in Fig. 11. It is clearly seen that the deposited particles have experienced severe plastic deformation to be a splat and the equiaxed grains have been elongated as shown in Fig. 11(b). When observed carefully in Fig. 11(b), it can be found that there are black inclusions at the interfaces of the particles, and these inclusions could

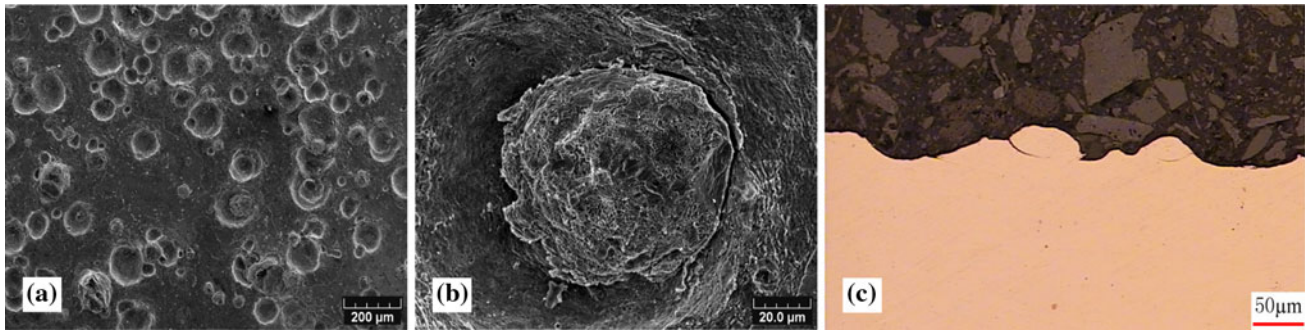

Fig. 9 Surface morphologies of the oxidized Cu (a, b) and cross section (c) after a single impact at 513 °C/2.7 MPa

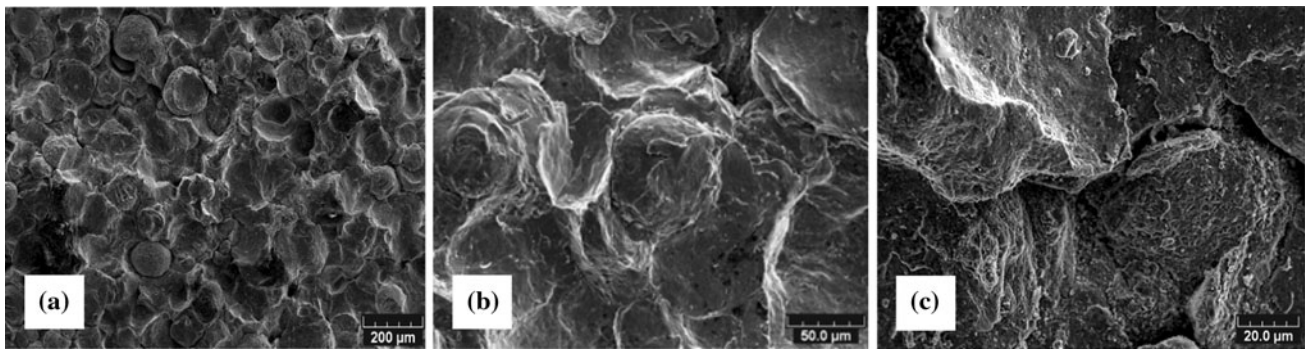

Fig. 10 Surface morphology of the coating with the oxidized Cu powder at 640 °C/2.5 MPa

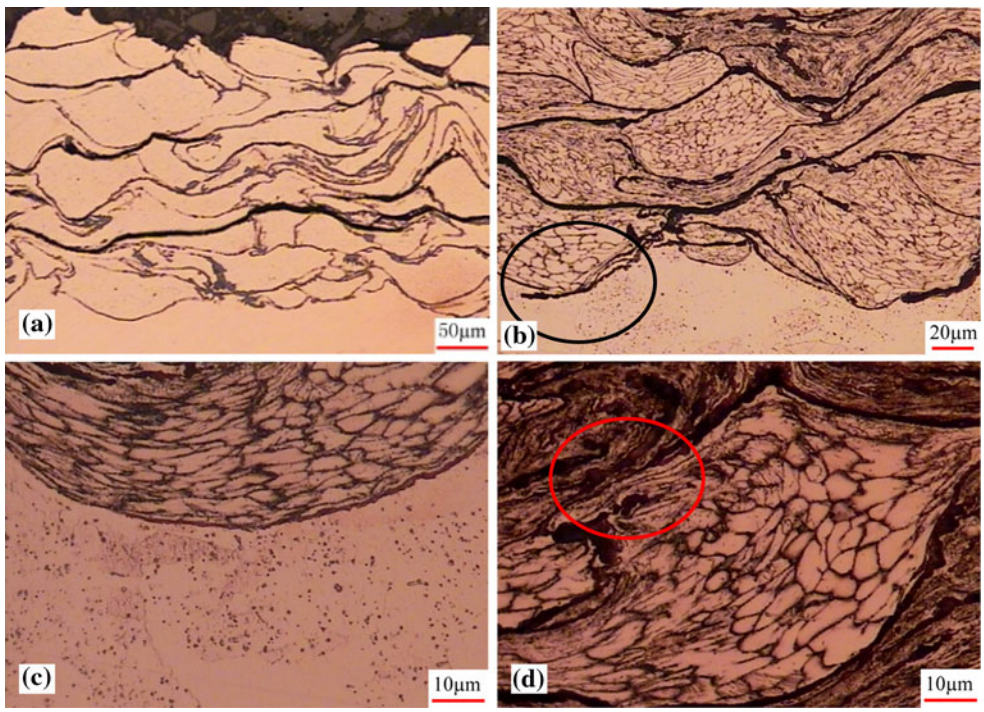

Fig. 11 OM of cross sections of coatings with the oxidized Cu powder before (a) and after (b, c, d) etching

result in the decrease of effective contact and a lower bonding strength between the coating and substrate (Ref 9). These phenomena further verify the most prevailing bonding hypothesis of the break-up and extrusion processes of the oxide films during CS illustrated in the literature (Ref 9). As the particle impinges upon the substrate, the plastic

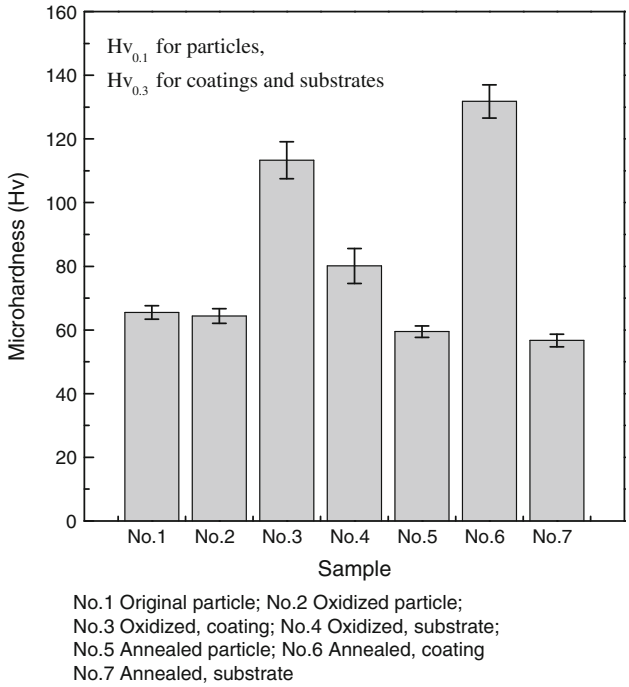

Fig. 12 Microhardness of particles, coating, and substrate

deformation disrupts the thin surface oxide films and extrudes them outward along the interface; however, most of them may be retained, providing intimate conformal contact under high local pressure with large enough deformation to permit bonding to occur. As is the case in the present study, more oxide films covering the oxidized Cu powder needs more kinetic energy to break them up and extrude them out, and thus higher kinetic energy is needed for bonding. After changing the gas condition from 513 °C/2.7 MPa to 640 °C/2.5 MPa, a thin coating can be formed with the oxidized Cu powder. Although changing the gas condition produces the same particle velocity, the higher particle temperature still decreases the critical velocity of the oxidized Cu powder; therefore, the oxidized particles can attain a plastic deformation comparable to that of the annealed particles.

3.3 Microhardness

The particle properties could also influence the particle deposition behavior (Ref 4), and therefore, the microhardness of the powders and coatings were investigated as shown in Fig. 12. By comparing these three samples of the starting particles (No. 1), the oxidized particles (No. 2), and the annealed particles (No. 5), it is found that the oxidized particles have a similar hardness to that of the starting particles but higher hardness than the annealed particles. In a similar way, it is seen that the hardness of the oxidized substrate (No. 4) is higher than that of the annealed Cu substrate (No. 7), which suggests that the annealing process released the strain and reduced the hardness of the particle and substrate. Thus, the higher hardness of the oxidized particles could be a reason for less deformation. Correspondingly, it is clearly seen that the deposited oxidized and annealed coatings (No. 3 and No. 6) show much higher hardness than the oxidized substrate (No. 4) and the annealed Cu substrate (No. 7), respectively, because of the strain-hardening effect by the high impact of particles during CS (Ref 10, 17). On the other hand, it is noticed that the hardness of the coating deposited with the oxidized powder (No. 3) is a little lower than that with the annealed powder (No. 6). It could be considered that the presence of the oxide films dissipates the kinetic energy and thus induces the inferior particle plastic deformation and impairs the strain-hardening effect, while the annealing treatment softens the particles and is beneficial to particle deformation, and thus the strain-hardening effect on the hardness of the annealed coating is superior to that of the oxidized coating in the present study.

4. Conclusions

Few oxidized particles could adhere to the substrate after a single impact, and correspondingly, a coating was hard to form at the gas condition of 513 °C/2.7 MPa, at which the annealed Cu coatings could be formed. After changing the gas condition to be 640 °C/2.5 MPa, a thin coating could be formed with the oxidized Cu powder because of the decrease of the critical velocity of the particle. SEM morphologies of the collected oxidized Cu powder revealed that the superior deformation occurring at the gas condition of 640 °C/2.5 MPa was the main reason. In addition, measurements of the oxygen content showed that the oxygen content of the collected powder after deposition at the gas condition of 640 °C/2.5 MPa was 0.23 wt.% compared to 0.63 wt.% in the starting oxidized powder. The results suggest that the rebounded particles have experienced large plastic deformation that results in the break-up of the oxide films during the impacting process. Correspondingly, the hardness of the coating deposited with the oxidized powder is a little lower than that with the annealed powder because of its inferior plastic deformation and strain-hardening effect, even if the oxidized powder exhibits a superior hardness to that of the annealed powder.

Acknowledgments

The authors would like to gratefully acknowledge the financial supports from the National Natural Science Foundation of China (51005180), the Fok Ying-Tong Education Foundation for Young Teachers in the Higher Education Institutions of China (131052), the Research Fund of the State Key Laboratory of Solidification Processing (NPU, China) (69-QP-2011), and the 111 Project (B08040).

References

1. A. Papyrin, Cold Spray Technology, *Adv. Mater. Process.*, 2001, **159**(9), p 49-51

2. C.K.S. Moy, J. Cairney, G. Ranzi, M. Jahedi, and S.P. Ringer, Investigating the Microstructure and Composition of Cold Gas-Dynamic Spray (CGDS) Ti Powder Deposited on Al 6063 Substrate, *Surf. Coat. Technol.*, 2010, **204**(23), p 3739-3749
3. H. Fukanuma, N. Ohno, B. Sun, and R.Z. Huang, In-flight Particle Velocity Measurements with DPV-2000 in Cold Spray, *Surf. Coat. Technol.*, 2006, **201**(5), p 1935-1941
4. H. Assadi, F. Gartner, T. Stoltenhoff, and H. Kreye, Bonding Mechanism in Cold Gas Spraying, *Acta Mater.*, 2003, **51**(15), p 4379-4394
5. C.J. Li, W.Y. Li, and H.L. Liao, Examination of the Critical Velocity for Deposition of Particles in Cold Spraying, *J. Therm. Spray Technol.*, 2006, **15**(2), p 212-222
6. T. Schmidt, F. Gartner, H. Assadi, and H. Kreye, Development of a Generalized Parameter Window for Cold Spray Deposition, *Acta Mater.*, 2006, **54**(3), p 729-742
7. W.Y. Li, H.L. Liao, C.J. Li, H.S. Bang, and C. Coddet, Numerical Simulation of Deformation Behavior of Al Particles Impacting on Al Substrate and Effect of Surface Oxide Films on Interfacial Bonding in Cold Spraying, *Appl. Surf. Sci.*, 2007, **253**(11), p 5084-5091
8. K. Kang, S. Yoon, Y. Ji, and C. Lee, Oxidation Dependency of Critical Velocity for Aluminum Feedstock Deposition in Kinetic Spraying Process, *Mater. Sci. Eng. A*, 2008, **486**(1-2), p 300-307
9. W.-Y. Li, C.-J. Li, and H. Liao, Significant Influence of Particle Surface Oxidation on Deposition Efficiency, Interface Microstructure and Adhesive Strength of Cold-Sprayed Copper Coatings, *Appl. Surf. Sci.*, 2010, **256**(16), p 4953-4958
10. T. Stoltenhoff, J. Voyer, and H. Kreye, Cold Spraying: State of the Art and Applicability, *International Thermal Spray Conference*, E. Lugscheider and C.C. Berndt, Eds., Essen, 2002, p 366-374
11. F. Gärtner, T. Stoltenhoff, T. Schmidt, and H. Kreye, The Cold Spray Process and Its Potential for Industrial Applications, *Thermal Spray Connects: Explore Its Surfacing Potential*, E. Lugscheider, Ed., DVS Deutscher Verband fur Schweißen, Basel, 2005, p 158-163
12. D.L. Gilmore, R.C. Dykhuizen, R.A. Neiser, T.J. Roemer, and M.F. Smith, Particle Velocity and Deposition Efficiency in the Cold Spray Process, *J. Therm. Spray Technol.*, 1999, **8**(4), p 576-582
13. C.J. Li, H.T. Wang, Q. Zhang, G.J. Yang, W.Y. Li, and H.L. Liao, Influence of Spray Materials and Their Surface Oxidation on the Critical Velocity in Cold Spray, *J. Therm. Spray Technol.*, 2010, **1-2**(19), p 95-101
14. W.-Y. Li, H. Liao, G. Douchy, and C. Coddet, Optimal Design of a Cold Spray Nozzle by Numerical Analysis of Particle Velocity and Experimental Validation with 316L Stainless Steel Powder, *Mater. Des.*, 2007, **28**(7), p 2129-2137
15. W.Y. Li, X.P. Guo, M. Yu, H.L. Liao, and C. Coddet, Investigation of Impact Behavior of Cold-Sprayed Large Annealed Copper Particles and Characterization of Coatings, *J. Therm. Spray Technol.*, 2011, **20**(1-2), p 252-259
16. M. Grujicic, C.L. Zhao, W.S. DeRosset, and D. Helfritch, Adiabatic Shear Instability Based Mechanism for Particles/Substrate Bonding in the Cold-Gas Dynamic-Spray Process, *Mater. Des.*, 2004, **25**(8), p 681-688
17. W.Y. Li, C.J. Li, and H.L. Liao, Effect of Annealing Treatment on the Microstructure and Properties of Cold-Sprayed Cu Coating, *J. Therm. Spray Technol.*, 2006, **15**(2), p 206-211